J Comput Aided Mol Des (2010) 24:57–75
DOI 10.1007/s10822-009-9314-z

A comparative study of AutoDock and PMF scoring performances, and SAR of 2-substituted pyrazolotriazolopyrimidines and 4-substituted pyrazolopyrimidines as potent xanthine oxidase inhibitors

Hamed I. Ali · Takayuki Fujita · Eiichi Akaho · Tomohisa Nagamatsu

Received: 16 August 2009 / Accepted: 4 December 2009 / Published online: 29 December 2009

Abstract 4-Alkylidenehydrazino-1H-pyrazolo[3,4-d]pyrimidines, 4-arylmethylidenehydrazino-1H-pyrazolo[3,4-d]pyrimidines, and 2-substituted 7H-pyrazolo[4,3-e]-1,2,4-triazolo-[1,5-c]-pyrimidines as potential xanthine oxidase inhibitors were docked into the active site of the bovine milk xanthine dehydrogenase using two scoring functions involved in AutoDock 3.05 and the CAChe 6.1.10. The correlation coefficiency obtained between the AutoDock binding energy and IC_{50} of the inhibitors was better than that obtained by the CAChe-PMF docking score. Many ligands exhibited one to four hydrogen bonds within the active site, where the detected hydrogen bonds by CAChe was identified quantitatively in the docked conformation by using MOPAC 2002. These ligands were docked into a long, narrow channel of the enzyme leading to the molybdopterin active moiety, with hydrogen bonding and electrostatic interaction between the planar aromatic moiety of the ligand and the enzyme. Furthermore, SAR among inhibitors was investigated, which revealed that the oxo group of pyrazolopyrimidine analogs is essential for its activity and the tricyclic derivatives are shown to be more potent than bicyclic ones. The mode of interaction of the docked inhibitors was described in details.

H. I. Ali · T. Fujita · T. Nagamatsu
Division of Pharmaceutical Sciences, Graduate School of Medicine, Dentistry and Pharmaceutical Sciences, Okayama University, 1-1-1 Tsushima-Naka, Okayama 700-8530, Japan

E. Akaho (✉)
Faculty of Pharmaceutical Sciences, Center for Area Research and Development (CARD), Kobe Gakuin University, 1-1-3 Minatojima, Chuo-ku, Kobe 650-8586, Japan
e-mail: akaho@pharm.kobegakuin.ac.jp

Keywords Pyrazolopyrimidine · Xanthine oxidase inhibitor · Structure activity relationship · AutoDock · PMF · CAChe

Introduction

During the course of our research group's work on the synthesis and biological evaluation of novel fused pyrimidines and purines, we found that 6-substituted 4-alkylidenehydrazino-1H-pyrazolo [3,4-*d*] pyrimidines, 4-aryl-methylidene hydrazino-1H-pyrazolo[3,4-*d*]pyrimidines, and 2-substituted 7H-pyrazolo [4,3-*e*]-1,2,4-triazolo-[1,5-*c*]-pyrimidines exhibited more potent bovine milk xanthine oxidase (XO) inhibitions than that of allopurinol in vitro [1–5]. Xanthine oxidoreductase accelerates the hydroxylation of a wide variety of purines, pyrimidine, and pterin substrates. In humans, the enzyme catalyzes the last two steps of purine catabolism, the oxidation of hypoxanthine to xanthine and of xanthine to uric acid (Scheme 1). This reaction occurs at a molybdenum-pterin center where the electrons are transferred via two Fe_2S_2 clusters to the isoalloxazine ring of FAD, which then passes them onto the second substrate NAD^+ [6]. No clinically more effective XO inhibitors for the treatment of hyperuricemia have been developed other than allopurinol, an analogue of hypoxanthine which was introduced for clinical use in 1963 by Elion et al. [7]. Because of shortcomings of allopurinol, new more potent inhibitors are under clinical investigation [8–16].

The use of xanthine oxidase inhibitors is not limited to hyperuricemia and gout. It has been shown that they can be used to treat cardiovascular diseases [17]. Many investigations have demonstrated the evidence of a strong correlation between urate levels and cardiovascular diseases

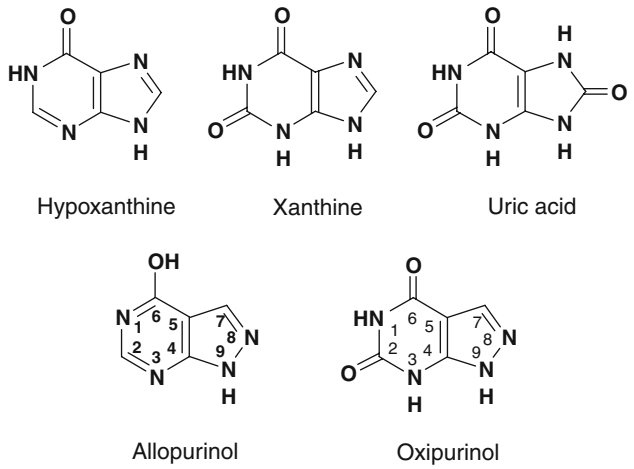

Scheme 1 Structure comparison of xanthine and its derivatives

[18]. Xanthine oxidase not only forms urate, but also catalyzes the formation of reactive oxygen species. High levels of reactive oxygen species are obviously linked to the worsen outcome in a variety of cardiovascular conditions. Allopurinol has been shown to improve endothelial dysfunction, reduce oxidative stress burden and modify myocardial efficiency by reducing oxygen consumption [19]. As for the physiological standpoint, oxygen plays predominant role in ATP generation, namely, oxidative phosphorylation. Reactive oxygen species including superoxide anion and hydrogen peroxide are produced as byproducts during this process. The over-production of reactive oxidative species induces in the initiation and progression of such diseases as cardiovascular disorder, inflammation, hypertension, viral pathogenesis, and ischemia–reperfusion [20]. To conclude the discussion of the current issue based on the literature review, it is reasonable to say that diseases caused by reactive oxygen species can be treated by the use of xanthine oxidative inhibitors whose therapeutic scope has been proved to expand.

Molecular modeling works on XO have been reported in the literature previously. Lin et al. [21] studied structure–activity relationship of coumarin derivatives on XO in terms of inhibiting and free radical-scavenging activities. They reported that the results of the structure-based molecular modeling exhibited interactions between coumarins and the molybdopterin region of XO and that the carbonyl pointed toward the Arg880, and the ester O atom formed hydrogen bonds with Thr1010. Prusis et al. [22] studied quantitative structure activity of hydrazones of *N*-amino-*N*′-hydroxyguanidine by measuring electron acceptor capacities for xanthine oxidase. They divided molecules into two groups one with nitro groups and the other without nitro groups based on the manual inspection of the structure–activity data. It was found that for set A molecules the presence of a nitro substituent at a certain distance range for the hydroxuguanidino group was most important and for set B molecules the acceptor activity was most influenced by the geometry of methoxy groups. Lin et al. [23] conducted a molecular modeling study of flavonoids and found that all of the tested flavonoids were competitive XO inhibitors and apigenin was the most potent inhibitor for its bicyclic benzopyranone ring to be tacked with phenyl of Phe 914.

In the present article, we report scoring performances of AutoDock and PMF when xanthine oxidase inhibitors are docked into the active site of the bovine milk dehydrogenase by using them. Another objective of this study is to investigate the structure–activity relationship between the inhibitory features of various ligands and the different docking energies including the experimentally measured xanthine oxidase inhibitory activity (IC_{50}) and the binding free energy (ΔG_b) calculated by AutoDock.

Background and objectives

Comparison of AutoDock and PMF scoring functions

A molecular docking is to achieve an optimized conformation for both the protein and ligand such that the free energy of the overall system is minimized. When used prior to the experimental screening, the molecular docking, can be as a powerful computational tool to reduce the labor and cost of drug development.

The genetic algorithm for ligand–protein docking was utilized by Olson's group as AutoDock. AutoDock is one of the most widely used docking programs in computational binding studies, which enables us to predict an optimized protein–ligand conformation with reasonable accuracy and speed. In AutoDock, the overall docking energy of a given ligand molecule in its active site is expressed as follows:

$$\begin{aligned}\Delta G^{\mathrm{aq}}_{\mathrm{bind}} = {} & W_{\mathrm{vdW}} \sum_{i=1} \sum_{j>i} \left(\frac{A_{ij}}{r_{ij}^{12}} - \frac{B_{ij}}{r_{ij}^{6}} \right) + W_{\mathrm{hbond}} E(t) \left(\frac{C_{ij}}{r_{ij}^{12}} - \frac{D_{ij}}{r_{ij}^{10}} \right) \\ & + W_{\mathrm{elec}} \sum_{i=1} \sum_{j>i} \frac{q_i q_j}{\varepsilon(r_{ij}) r_{ij}} + W_{\mathrm{tor}} N_{\mathrm{tor}} \\ & + W_{\mathrm{sol}} \sum_{i=1} \sum_{j>i} \left(S_i V_j + S_j V_i \right) e^{\left(-r_{ij}^2 / 2\sigma^2 \right)}\end{aligned} \tag{1}$$

In Eq. 1, W_{vdW}, W_{hbond}, W_{elec}, W_{tor}, and W_{sol} are weighting factors of van der Waals, hydrogen bond, electrostatic interactions, torsional term, and desolvation energy of protein–ligand complex, respectively. r_{ij}, A_{ij}, B_{ij}, C_{ij}, and D_{ij} represent the interatomic distance, the depths of energy well, and the equilibrium separations between the two atoms, respectively.

As shown in Eq. 1, the first three terms are in vacuo force field energies for intermolecular interactions. The fourth term accounts for the internal steric energy of the ligand molecule. All these terms are taken from the AMBER theory [24]. The CAChe molecular modeling program automates the docking of a ligand into the active site by using a genetic algorithm with a fast simplified potential of mean force (PMF) [25]. PMF is a knowledge-based scoring approach based on the work of Muegge et al. [26–28]. The PMF score is calculated as a sum of over all atom pair interaction free energies between the protein and ligand. $A_{ij}(r)$ represents a scoring function of the atom pair with distance r. In Eq. 2, kl is a protein–ligand atom pair of type ij.

$$\text{PMF\_score} = \sum_{\substack{kl \\ r < r^{ij}_{\text{cut-off}}}} A_{ij}(r) \qquad (2)$$

One of the advantages of CAChe is to offer us a relatively unbiased searching. The docking calculation for CAChe is performed by the FastDock computing engine. Similar to AutoDock, FastDock uses a Lamarckian GA in which a minimization is achieved so that docking populations adapt themselves to the environment in which they are placed.

Herein we report a series of investigations of docking and scoring of various pyrazolopyrimidines ligands of potential activities against two xanthine dehydrogenases (XDH) from bovine milk, one with inhibitor TEI-6720 bound (PDB code: 1n5x) and the other with inhibitor FYX-051 bound (PDB code: 1v97) [29, 30]. In this study, both AutoDock as an empirical docking method and CAChe-PMF as a knowledge-based scoring function were investigated. Furthermore, a comparative study was carried out for the performance of these two methods focused on the AutoDock binding free energy and the PMF docking score, respectively.

Previous investigations on scoring functions

Wang et al. tested eleven scoring functions to evaluate their abilities to reproduce experimentally determined structures. Those functions include four scoring functions implemented in the LigFit module in Cerius 2 (PMF, LigScore, PLP, and LUDI), four scoring functions implemented in the CScore module in SYMYL (*F*-Score, *G*-Score, *D*-Score, and ChemScore), the scoring function implemented in the AutoDock, and two stand-alone scoring functions (DrugScore, and *X*-Score) [24]. They inspected how closely the best-scored (or the lowest energy) docked conformation predicted by each scoring function resembles the one observed in the experimental complex structure for the evaluation of a scoring function in terms of docking accuracy. By using the AutoDock scoring function (success rate = 62%) as reference, it was found that six scoring functions (PLP, *F*-Score, LigScore, DrugScore, LUDI, and *X*-Score) gave better results (success rates ranging from 66 to 76%), while the other four scoring functions (PMF, *G*-Score, Chem-Score, and *D*-Score) did not (success rates ranging from 26 to 52%).

Ferrari et al. reported the results of an extensive study on a series of 28 inhibitors of aldose reductase with experimentally determined crystal structures and inhibitory activities, in which they evaluated the ability of the molecular mechanics Poisson-Boltzmann surface area (MM-PBSA) and the molecular mechanics generalized Born surface area (MM-GBSA) methods in predicting biding free energies using a number of different simulation conditions [31]. They found that MM-PBSA proved to perform better than MM-GBSA, and within the MM-PBSA methods, the PBSA of Amber performed similarly to Delphi. Warren et al. evaluated 10 docking programs (Dock4, DockIt, FlexX, Flo, Fred, Glide, Gold, LigFit, MOE, and MVP) against eight proteins of seven protein types for three tasks: binding mode prediction, virtual screening for lead identification, and rank-ordering by affinity for lead optimization. They found that all of the docking programs were able to generate ligand conformations similar to crystallographically determined protein/ligand complex structures for at least one of the targets, although scoring functions were less successful at distinguishing the crystallographic conformation from the set of docked poses [32]. de Graaf et al. found that the consideration of water molecule at predicted positions in the active site and the rescoring of pooled docking poses from four different docking programs (AutoDock, FlexX, GOLD-Goldscore, and GOLD-Chemscore) with the SCORE scoring function enabled the successful prediction of experimentally reported sites of catalysis of more than 80% of the substrates [33]. We have learned from the previous investigations of performances and validations of various docking programs that the docking results depend on the types of proteins and inhibitors in question, the medicinal characteristics of the study, and the database coverage. Hence, we need to evaluate the docking results based on the specific needs of our investigation.

Results and discussion

Validation of the accuracy and performance of AutoDock and PMF scoring functions

The most straightforward method for the validation of scoring functions is to inspect how closely the best-scored docked conformation resembles the bound ligand in the experimental crystal structure. As cited in the literature, if

the RMSD (root mean square deviation) of the best docked conformation is ≤2.0 Å from the experimental crystal position of the ligand, this docking performance is considered to be reasonably successful [24]. Therefore, in order to validate the reliability of the docking performances and accuracies of AutoDock 3.05 and CACHe 6.1.10, the original bound ligands **TEI-6720**, "2-(3-cyano-4-isobutoxy-phenyl)-4-methyl-5-thiazole-carboxylic acid" and **FYX-051**, "4-(5-pyridin-4-yl-1H-1,2,4-triazol-3-yl) pyridine-2-carbonitrile" were separated and docked into their corresponding bovine milk xanthine dehydrogenases (XDH; 1n5x and 1v97), respectively. And then the docked results were compared to the experimentally determined crystal structure of the bound ligand–protein complex.

The obtained success rates of AutoDock 3.0.5 and CACHe 6.1.10 were fairly well as shown in Figs. 1 and 2, respectively. For the docking of the TEI ligand against XDH (1n5x) by using AutoDock, the RMSD values for the obtained three conformations were 0.633, 0.659, and 0.197 Å, with binding free energies of ΔG_b: −10.34.

For the docking of the TEI and FYX ligands against XDH (1n5x and 1v97) using CACHe 6.1.10, it is clearly noticed that the docked ligands were exactly superimposed with the experimentally determined crystal structure position with high binding affinities (PMF binding scores: −109.17 and −107.85 kcal/mol, and RMSD: 0.625 and 0.275 Å, respectively). Moreover, the docked TEI ligand exhibited three hydrogen bonds with Arg 880 and Thr 1010, which are exactly the same amino acids as those involved in the experimentally determined crystal structure ligands. These docking results indicate that AutoDock and CACHe performance proved to be reliable, efficient and accurate to some extents in predicting binding modes observed by X-ray co-crystals of XDH [29, 30]. These docking performances would provide information valuable to validate the further docking studies of our in silico synthesized compounds.

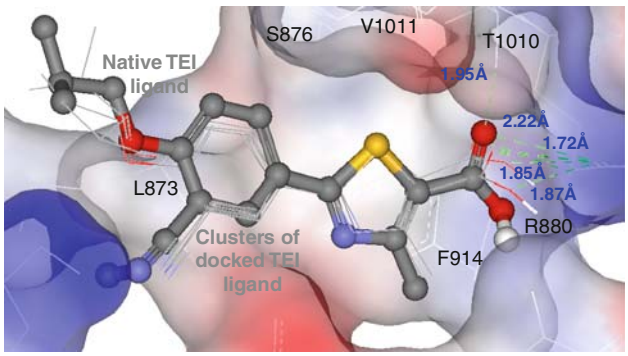

Rank	ΔG_b (kcal/mol)	Run	No. in cluster	Docking Histogram 5 10 15 20 25 30 35	RMSD (Å)
1	−1034	2	37	##	0.633
2	−10.34	1	12	############	0.659
3	−10.31	26	1	#	0.197

Fig. 1 The different conformational clusters of TEI ligand (shown as *lines*, colored by elements) docked into the binding site of XDH (1n5x). The docked ligands were exactly superimposed on the embedded, experimental ligand (shown in *ball* and *stick*, colored by elements) with RMSD of 1.97–0.659 Å as illustrated in the attached docking histogram. All of ligands were bound by hydrogen bonds (*green dotted lines*) which involved exactly the same amino acids as in the crystal structure of XDH. The binding free energies of each cluster are shown in the increasing order, −10.34 kcal/mol, −10.34 kcal/mol, and −10.2 kcal, respectively

Docking of the pyrazolopyrimidine derivatives against XDH (1n5x and 1v97)

A comparative evaluation of the scoring functions of AMBER force fields pertaining to AutoDock 3.05 and PMF involved in CACHe 6.1.10 was undertaken. This type of study attracts attention of many researchers in this field since both of these scoring functions have been widely used in structure-based drug design.

Each of the 52 structures of the bicyclic pyrazolopyrimidines, and the tricyclic pyrazolotriazolopyrimidines (Scheme 2) whose IC_{50} against XO enzymes are known (Table 1), was docked against the XDH (1n5x and 1v97). The analysis of the data was performed by evaluation of RMSD, hydrogen bond and visual comparison of the obtained coordinates relative to the crystallographic coordinates used as reference. Table 1 lists the best docking data obtained for the pyrazolopyrimidines against XDH (1n5x) by AutoDock. These data include binding free energies, estimated inhibition constants, hydrogen bonds, and RMSD of the best top ranked conformations of the docked inhibitors.

Most of the proposed binding modes by AutoDock produced RMSDs less than 6.0 Å (1.21–5.59 Å), with more than one-third of these conformations being less than 3 Å compared to the X-ray structure position. As cited in Table 1, AutoDock binding free energies (ΔG_b), as an important docking parameter, were obtained for the docked bicyclic pyrazolopyrimidines in the range of −11.85 to −7.72 kcal/mol whereas docked poses with binding free energies (ΔG_b) of less than −9.23 kcal/mol amounted to 79%, and for the tricyclic pyrazolotriazolopyrimidines, in the range of ΔG_b: −11.78 to −8.86 kcal/mol whereas of less than −10.0 kcal/mol, to 79%. These results are proportionally represented their IC_{50} values of xanthine oxidase inhibitory activities in the range of 0.077–7.89 and 0.032–0.782 μM, respectively, except for compound **3l** whose IC_{50} was more than 10 μM (this value may be inaccurate because the compound was insoluble in DMSO). By comparing these results with those of the positive controls, oxipurinol (IC_{50}: 22.1 μM; ΔG_b:

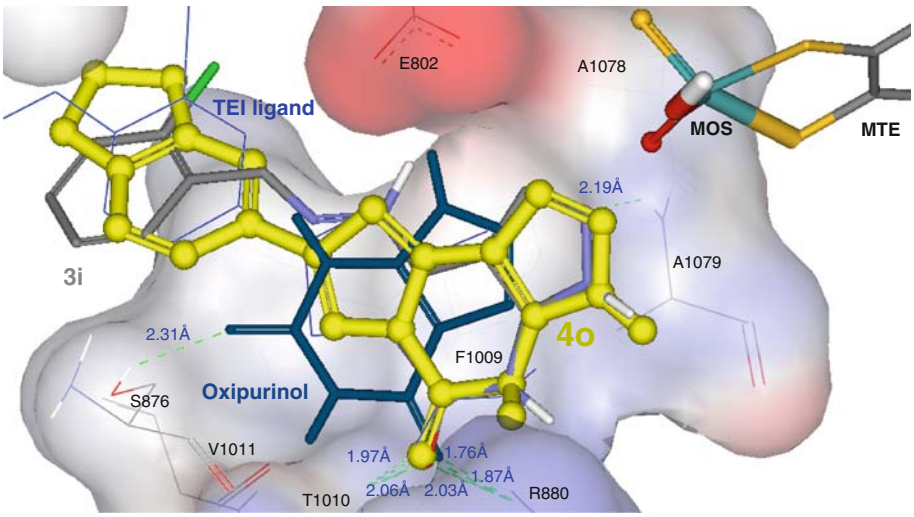

Fig. 2 The comparative binding interaction features of oxipurinol (*indigo*, *stick*), pyrazolopyrimidine (**3i**, colored by elements, *stick*), and the pyrazolotriazolopyrimidine (**4o**, *yellow*, *ball* and *stick*) docked into the binding site of XDH (1n5x) using AutoDock3.05. Ligands were oriented by their N_2–N or N_8–N interaction near to the dioxothiomolybdenum (MOS) moiety, forming two to three hydrogen bonds (shown in *green dotted lines*) involving mainly Thr1010 and Arg880

Scheme 2 Structures of different bicyclic pyrazolopyrimidines (**1**–**3**) and tricyclic pyrazolotriazolopyrimidines (**4a**–**s**) obtained in the docking investigation into the active site of XDH (PDB codes: 1n5x and 1v97)

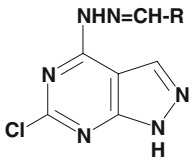

1a-g

4-Aldehydehdrazones of 6-chloropyrazolo[4,3-*d*]pyrimidines

1,2 a: R = *n*-C_7H_{15}
b: R = Ph
c: R = 4-F-C_6H_4
d: R = 4-Cl-C_6H_4
e: R = 4-Me-C_6H_4
f: R = 4-MeO-C_6H_4
g: R = 4-O_2N-C_6H_4

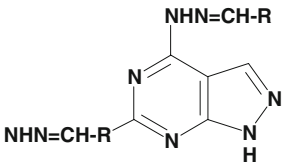

2a-g

4,6-Bis-aldehydehdrazones of pyrazolo[4,3-*d*]pyrimidines

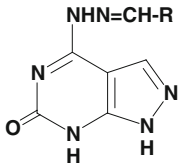

3a-s

4-Alkylidenehydrazino- and 4-arylmethylidenehydrazino-1*H*-pyrazolo[4,3-*d*]pyrimidin-6(7*H*)-ones

3,4 a: R = H
b: R = Me
c: R = Et
d: R = *n*-Bu
e: R = *n*-C_7H_{15}
f: R = CH_2=CH-$(CH_2)_8$
g: R = Ph
h: R = 4-F-C_6H_4
i: R = 2-Cl-C_6H_4
j: R = 3-Cl-C_6H_4
k: R = 4-Cl-C_6H_4
l: R = 4-Br-C_6H_4
m: R = 4-Me-C_6H_4
n: R = 4-MeO-C_6H_4
o: R = 3,4-OCH_2O-C_6H_3
p: R = 4-HOOC-C_6H_4
q: R = 4-HO-C_6H_4
r: R = 4-O_2N-C_6H_4
s: R = 3-O_2N-4-HO-C_6H_4

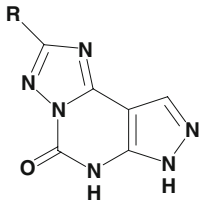

4a-s

7*H*-pyrazolo[4,3-*e*]1,2,4-triazolo [1,5-*c*]pyrimidin-5(6*H*)-one

−7.54 kcal/mol), allopurinol (IC_{50}: 24.3 μM; ΔG_b: −7.39 kcal/mol), and the extremely potent XO inhibitor, TEI bound ligand obtained from PDB with PDB code of 1n5x (IC_{50}: 0.0014 μM [16]; ΔG_b: −10.34 kcal/mol). It is noticed that there is a good correlation between the AutoDock binding free energy and the biological activity. This correlation may be helpful for further structure-based design of pyrazolopyrimidine xanthine oxidase inhibitors.

As far as H-bond is concerned, some reports say that the H-bond distance can be greater than 3.2 Å [30, 34]. However, in this study H-bonds distances less than 2.5 Å are considered to be relevant as the relatively longer H-bonds in distance are too weak to argue for our study purpose. Also the ideal hydrogen bond should have an angle θ of 180° between the acceptor atom and the donor atom. Thus, as an angle θ decreases, the strength of the hydrogen bond is reduced. No hydrogen bonds exist when angle θ is 90° or less. Therefore, it is suffice to say that hydrogen bonds with the angle $\theta \geq 135°$ are sufficiently strong.

Table 1 The best docking results based on the binding free energies (ΔG_b) of the compounds docked against XDH (PDB code: 1n5x), the distance and angle of hydrogen bonds between compounds and amino acid residues involved in XDH, and RMSD from the crystallized TEI-6720 ligand

Compound	IC_{50} (μM)[a]	ΔG_b (kcal/mol)[b]	Hydrogen bonds between atoms of compounds and amino acids				RMSD (Å)[d]
			Atom of compound	Amino acid	Distance (Å)	Angle (°)	
Allopurinol	24.3	−7.39	N_8–N	HN of Thr 1010	2.05	167.0	5.55
			C_6–OH	OE2 of Glu 802	2.17	155.5	
Oxipurinol	22.1	−7.54	C_2–Oxo	HO of Ser 876	2.31	146.7	3.93
			C_6–Oxo	HN of Thr 1010	2.06	135.4	
			C_6–Oxo	Hn(HH22) of Arg 880	1.76	162.8	
3a	–[d]	−7.72	C_6–Oxo	HN of Thr 1010	2.08	136.6	5.05
			C_6–Oxo	HN(HH22) of Arg 880	1.87	151.3	
3b	4.670	−8.07	N_7–H	OH of Thr 1010	2.19	138.9	3.90
			C_6–Oxo	HN(HH22) of Arg 880	1.71	146.1	
3c	–	−8.53	C_6–Oxo	HN(HH22) of Arg 880	1.72	141.5	4.38
3d	–	−9.23	N_2–N	HE of Arg 880	1.99	138.0	4.86
			N_2–N	HH22 of Arg 880	1.72	145.8	
3f	7.894	−9.34	C_6–Oxo	HN of Ala 1079	2.21	164.6	2.14
3g	0.305	−9.88	N_2–N	HN(HE) of Arg 880	2.27	135.9	4.83
			N_2–N	HN(HH22) of Arg 880	1.67	159.1	
			N_1–H	OH of Thr 1010	1.84	147.2	
3h	0.373	−9.35	N_2–N	HN Ala 1079	2.07	145.9	2.86
			C_4–NH	OE1 of Glu 802	1.86	136.1	
			C_6–Oxo	HN(HH22) of Arg 880	2.03	157.7	
			C_6–Oxo	HN of Thr 1010	1.90	141.1	
3i	0.077	−9.79	C_6–Oxo	HN of Thr 1010	2.05	137.3	3.08
			C_6–Oxo	HN(HH22) of Arg 880	1.87	153.8	
			N_2–N	HN of Ala 1079	2.19	148.8	
3j	0.223	−9.35	N_2–N	HN Ala 1079	2.27	147.5	3.10
			C_6–Oxo	HN(HH22) of Arg 880	1.83	150.8	
3k	0.224	−9.55	N_2–N	HN Ala 1079	2.22	143.4	2.93
			C_6–Oxo	HN(HH22) of Arg 880	2.06	155.3	
			C_6–Oxo	HN of Thr 1010	1.92	141.5	
3l[e]	>10	−10.39	C_6–Oxo	HN of Thr 1010	1.94	138.4	3.09
			C_6–Oxo	HN(HH22) of Arg 880	1.91	162.1	
			C_1–N	HN of Ala 1079	2.26	147.0	
3m	0.247	−10.34	C_6–Oxo	HN of Thr 1010	1.96	140.0	2.95
			C_6–Oxo	HN(HH22) of Arg 880	1.96	158.9	
			C_4–NH	OE1 of Glu 802	1.74	137.7	
			N_2–N	HN of Ala 1079	2.24	146.4	
3n	0.172	−9.91	C_6–Oxo	HN of Thr 1010	2.03	162.6	2.94
			C_6–Oxo	HN(HH22) of Arg 880	2.05	154.7	
3o	0.385	−10.96	C_6–Oxo	HN of Thr 1010	2.08	143.0	3.04
			C_6–Oxo	HN(HH22) of Arg 880	2.07	152.8	
			N_2–N	HN of Ala 1079	1.97	144.6	
3p	0.399	−10.55	*p*–COO	HN(HZ1) of Lys 771	1.99	145.2	2.14
			C_6–Oxo	HN(HH22) of Arg 880	1.92	171.0	
			N_2–N	HN of Ala 1079	2.23	152.6	
3q	0.359	−9.81	C_6–Oxo	HN of Thr 1010	2.07	143.4	2.82
			C_6–Oxo	HN(HH22) of Arg 880	2.13	150.8	

Table 1 continued

Compound	IC_{50} (μM)[a]	ΔG_b (kcal/mol)[b]	Hydrogen bonds between atoms of compounds and amino acids				RMSD (Å)[d]
			Atom of compound	Amino acid	Distance (Å)	Angle (°)	
3r	1.925	−10.23	*p*–N=O	HN(HE) of Arg 880	2.14	137.5	1.21
			p–N=O	HN(HH22) of Arg 880	2.49	139.1	
			p–N=O	HN of Thr 1010	1.71	155.1	
			p–N^+–O^-	HN(HH22) of Arg 880			
3s	–	−11.85	C_6–Oxo	HN of Thr 1010	1.88	143.2	2.16
			C_6–Oxo	HN(HH22) of Arg 880	2.12	156.3	
			N_2–N	HN of Ala 1079	2.07	143.1	
4a	0.184	−8.86	C_5–Oxo	HH22 of Arg 880	1.85	158.2	5.59
4b	0.250	−9.40	C_5–Oxo C_5–Oxo	HN of Thr 1010	1.96	138.2	5.35
				HN(HH22) of Arg 880	1.90	158.6	
4c	0.782	−9.33	C_5–Oxo	HN(HH22) of Arg 880	1.77	153.5	4.82
			N_8–N	HN of Ala 1079	2.24	147.0	
4d	0.529	−10.15	C_5–Oxo	HN(HH22) of Arg 880	1.83	138.2	4.32
			N_6–H	OH of Thr 1010	1.85	149.9	
4e	0.069	−10.84	C_5–Oxo	HN(HH22) of Arg 880	1.67	152.3	3.49
			N_8–N	HN of Ala 1079	2.33	146.7	
4f	0.117	−11.11	C_5–Oxo	HN(HH22) of Arg 880	1.87	136.2	2.27
			N_8–N	HN of Ala 1079	1.93	145.8	
4g	0.103	−10.53	C_5–Oxo	HN of Thr 1010	1.95	139.8	3.92
			C_5–Oxo	HN(HH22) of Arg 880	1.95	159.9	
			N_8–N	HN of Ala 1079	2.44	146.4	
4h	0.062	−10.68	C_5–Oxo	HN of Thr 1010	1.96	142.9	3.58
			C_5–Oxo	HN(HH22) of Arg 880	2.06	158.4	
4i	0.070	−10.90	C_5–Oxo	HN of Thr 1010	1.95	140.7	3.75
			C_5–Oxo	HN(HH22) of Arg 880	1.98	160.8	
4j	0.038	−11.21	C_5–Oxo	HN of Thr 1010	1.94	142.5	3.62
			C_5–Oxo	HN(HH22) of Arg 880	2.05	158.6	
4k	0.032	−10.97	C_5–Oxo	HN of Thr 1010	1.99	142.1	3.54
			C_5–Oxo	HN(HH22) of Arg 880	2.04	155.7	
4l	0.034	−11.08	C_5–Oxo	HN of Thr 1010	1.99	140.8	3.55
			C_5–Oxo	HN(HH22) of Arg 880	1.98	156.7	
			N_8–N	HN of Ala 1079	2.28	146.5	
4m	0.041	−10.98	C_5–Oxo	HN of Thr 1010	2.00	141.6	3.55
			C_5–Oxo	HN(HH22) of Arg 880	2.02	155.7	
			N_8–N	HN of Ala 1079	2.23	146.3	
4n	0.053	−10.60	C_5–Oxo	HN of Thr 1010	1.98	141.9	3.23
			C_5–Oxo	HN(HH22) of Arg 880	2.03	156.4	
			N_8–N	HN of Ala 1079	2.27	146.0	
4o	0.041	−10.89	C_5–Oxo	HN of Arg Thr 1010	1.97	144.1	2.88
			C_5–Oxo	HN(HH22) of Arg 880	2.03	157.3	
4q	0.055	−10.49	C_5–Oxo	HN of Arg Thr 1010	1.98	141.4	3.26
			C_5–Oxo	HN(HH22) of Arg 880	2.01	156.5	
			N_8–N	HN of Ala 1079	2.29	146.1	
4r	0.060	−11.19	C_5–Oxo	HN of Thr 1010	1.89	142.8	2.52
			C_5–Oxo	HN(HH22) of Arg 880	2.06	161.4	
			N_8–N	HN of Ala 1079	2.34	145.4	

Table 1 continued

Compound	IC_{50} (μM)[a]	ΔG_b (kcal/mol)[b]	Hydrogen bonds between atoms of compounds and amino acids				RMSD (Å)[d]
			Atom of compound	Amino acid	Distance (Å)	Angle (°)	
4s	0.037	−11.78	N_5–H	OH of Thr 1010	1.75	140.7	1.30

[a] Through reference 1

[b] Binding free energy

[c] Root mean square deviation

[d] Not determined

[e] This value is inaccurate because of the insolubility in DMSO

One to four hydrogen bonds were observed between the docked ligands and the binding site of XDH (1n5x). Those hydrogen bonds involved six different amino acids, namely Lys 771, Glu 802, Ser 876, Arg 880, Thr 1010, and Ala 1079. Arg 880 and Thr 1010 are the most commonly involved amino acids by those ligands. Similar to the binding modes of allopurinol by its N_8–N and C_4–OH atoms and oxipurinol by its C_2–oxo and C_6–oxo groups, all the given inhibitors were bound into the XDH pocket by their corresponding N_2–N and C_6–oxo atoms for bicyclic pyrazolopyrimidines and by N_8–N and C_5–oxo atoms for tricyclic pyrazolotriazolopyrimidines.

The binding modes and hydrogen bodings of oxipurinol, ligands **3i** and **4o** docked by AutoDock 3.05 took place deeply into the binding site of XDH (1n5x) as shown in Fig. 3. The bicyclic pyrazolopyrimidine (**3i**, IC_{50}: 0.077 μM) was docked into the groove of the binding site of XDH. The docking result showed that RMSD of the crystal structure of TEI ligand was 3.08 Å and three hydrogen bonds were observed involving Arg 880, Thr 1010, and Ala 1079. Similarly, the pyrazolotriazolopyrimidine (**4o**, IC_{50}: 0.041 μM) was docked forming two hydrogen bonds involving Arg 880 and Thr 1010, and it exhibited a smaller RMSD of 2.88 Å than that of the crystal structure of TEI ligand. Oxipurinol (IC_{50}: 22.1 μM) as positive control exhibited three hydrogen bonds with Ser 876, Arg 880, and Thr 1010 exhibiting RMSD of 3.93 Å. All of these docked conformations were bound closer to the buried Mo-pterin cofactor by their N_8–N (for oxipurinol), N_2–N (for **3i**) or N_8–N (for **4o**), with the distances of 3.18, 1.78, and 1.83 Å, respectively. This indicates that they block the activity of the enzyme sufficiently enough to prevent the substrate from binding to the active site. Experimentally these ligands exhibited potent inhibitory activities against bovine milk xanthine oxidase in vitro, from several times to several hundred times as potent as oxipurinol [1].

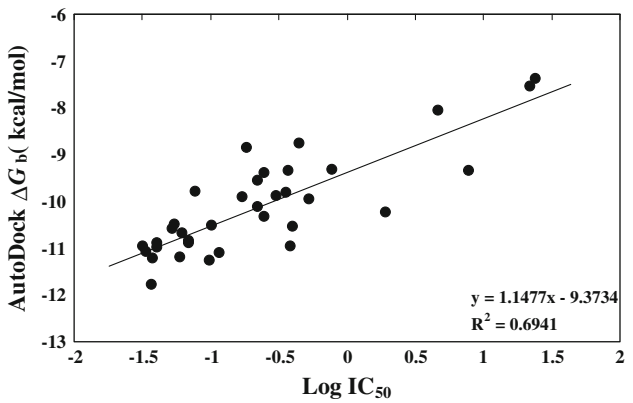

Fig. 3 A correlation feature between the AutoDock binding free energy (Δ*G*b) and log IC_{50} of allopurinol, oxipurinol, **3b**, **e**–**k**, **m**–**r**, and **4a**–**s** docked against XDH (1n5x)

As clearly demonstrated in Fig. 3, a significant good correlation was obtained between the AutoDock binding free energy (ΔG_b) and the log IC_{50} for 35 ligands including **3b**, **e**–**k**, **m**–**r**, and **4a**–**s** in addition to allopurinol and oxipurinol docked into XDH (1n5x). A good linearity and distribution of points on the regression line is shown with the standard deviation (SD) of 0.593, correlation coefficient (R^2) of 0.694, and probability value (p) of <0.0001 for the docked ligands (n) =35. Removing two outliers (compound **3f**, **r**) the improved correlation R^2 of 0.769 and the standard deviation of 0.5277 were obtained.

This result also demonstrates a fairly reasonable performance of scoring function involved in AutoDock 3.0.5 in silico simulation to correlate the experimental bioassay. Interestingly, it was shown that a good direct correlation was observed between the AutoDock binding free energies and XO inhibitory activities of **TEI-6720** (IC_{50}: 0.0014 μM, ΔG_b: −10.34 kcal/mol). Allopurinol and oxipurinol also revealed a good correlation between the docking and bioassay results against XDH (1n5x), that is, IC_{50}: 24.3 μM and ΔG_b of −7.39 kcal/mol, and IC_{50} of 22.1 μM and ΔG_b of −7.54 kcal/mol, respectively.

On the other hand, 4-aldehydedrazones of 6-chloropyrazolo[4,3-d]pyrimidines (**1a**–**g**) and 4,6-bis-aldehydedrazones of pyrazolo[4,3-d]pyrimidines (**2a**–**g**) did not show any appreciable inhibitory activities against xanthine oxidase, as $IC_{50's}$ > are greater than 10 μM for all of them [1].

Docking of these ligands against XDH (1n5x) by using AutoDock 3.05 revealed higher binding free energies i.e. lower binding affinities within the binding site, as they exhibited binding free energies of −9.52 to −8.04 kcal/mol. These low binding affinities are obviously attributed to the absence of a polar C_6–oxo group which is considered as key element for hydrogen bond formation in the binding site of XDH as cited for oxipurinol (C_2–oxo) and inhibitors **3** and **4** shown in Table 1. Moreover, the bulky 4,6-bis-aldehydedrazones of pyrazolo [4,3-d] pyrimidines (**2a**–**g**) compounds plays a role in producing lower binding affinities of these ligands in the binding site. Eventually, these docking features are reasonably consistent with the experimental bioassay results.

The standard PMF scoring function using CAChe was applied for docking of the 52 structures of the bicyclic pyrazolopyrimidines and the tricyclic pyrazolotriazolopyrimidines represented in Scheme 2. The PMF docking scoring function is related to the binding affinity, but it is not based on binding free energy. It usually shows energies many times larger than the binding free energy as indicated in Eq. 3 [35].

$$\Delta G_{\text{bind}} = \text{PMF}_{\text{score}}/\varepsilon \quad (3)$$

ε in Eq. 3 stands for all the varying terms involved in the scoring function. The parameters used were adjusted to be equivalent to those used in binding parameters of AutoDock. All data were obtained by docking of the different ligands into the crystal structure of TEI-6720 ligand. XDH (PDB code: 1n5x) is represented in Tables 2 and 3, including the PMF-docking scores, detected H-bonds by CAChe, and their length in Å, and the quantitative identification of the detected hydrogen bond by using the MOPAC 2002.

A docking simulation of ligands against the enzyme by using CAChe 6.1.10 revealed that many inhibitors were bound into XDH (1n5x and 1v97) creating one to four hydrogen bonds involving such amino acids as Asn 768, Glu 802, Ser 876, Arg 880, Thr 1010, Val 1011, and Ala 1079 in addition to the HET group, dioxothiomolybdenum (MOS). It is clearly shown that the docked molecules revealed smaller RMSD than those of AutoDock binding function. The overall RMSD involving XDH (1n5x) was 0.47–4.51 Å, 53% less than an average H-bond of 2.0 Å, and the RMSD involving XDH (1v97) was 0.32–1.45 Å, 73% less than an average H-bond of 2.0 Å. However, H-bonding in some of the highly potent pyrazolotriazolopyrimidine was not identified in bond order by MOPAC. This may be attributed to their rigid coplanar structure which prevents them from joining the polar moieties to form straight angle H-bonds. Many H-bonds of more than 2.5 Å in length, which are generally not considered as a genuine H-bond, and are expected to be weaker in binding and pseudo-type in nature. Docking runs with greater than 40,000 generations usually simulate better the actual ligand–protein interaction in vivo than otherwise. These planar compounds tend to interact with the protein active site with van der Waals, electrostatic and hydrophobic–hydrophobic interactions. As is seen in docking using the AutoDock binding energy function and the CAChe-docked energy function as well, Arg 880 and Thr 1010 were the most commonly involved amino acids in the hydrogen bond formation.

The extent of correlations of the docking scores between 1n5x and 1v97 obtained by the CAChe-PMF scoring function were similar as shown in Fig. 4. A reasonable distribution linearity of points on the regression line is reflected observed in Fig. 4a. It shows such values as standard deviation (SD): 10.416, correlation coefficient (R^2): 0.478 and probability value (p): <0.0001 involving 35 ligands. Removing two outliers (compound **3e**, **j**) improved the correlation R^2 to 0.542 and the standard deviation to 9.170. Similar results were obtained as shown in Fig. 4b for the docking of 1v97 against XDH (1v97) with the standard deviation (SD): 8.831, correlation coefficient (R^2): 0.496, and probability value (p): <0.0001 involving 35 ligands. Removing two outliers (compound **3f**, **m**) improved the correlation R^2 to 0.613 and the standard deviation to 7.607.

Interestingly enough, it was found that points between IC_{50} and the binding energy of AutoDock (Fig. 3) exhibited homogenous distributions around the regression line. This plot did not reveal drastic "false negatives" (active compounds that are scored too low) that would lie in the upper left quarter of the graph. It is crucial that no false negatives are generated in the virtual screening (VS) protocol in filtering out compounds of a database by computational simulation. A deviation from the optimal correlation region by "false negative" with CAChe PMF scoring functions was observed slightly more than by "false positive".

Therefore, comparatively speaking, the observation of these results of Muggue's PMF scoring approach involved in CAChe 6.1.10 showed that its performance is slightly poorer than that of AutoDock3.-05.

Docking of 4-phenylmethylidenehydrazino-1H-pyrazolo [3,4-*d*] pyrimidine-6(7H)-one (**3g**; IC_{50}: 0.305 μM) against XDH (1n5x) resulted in the docking score of −95.24 kcal/mol. It was deeply docked into the binding site showing two H-bonds, as shown in Fig. 5; one between hydrazine hydrogen of the ligand and oxygen of Glu 802 and the other between C_6–oxo of the ligand and hydrogen of Thr 1010. The existence of the former H-bond was confirmed by MOPAC. The docked ligand was oriented by its N_2–N atom within the distance of 3.45 Å of the dioxothiomolybdenum (MOS) moiety, indicating the high binding

Table 2 The best docking results based on the PMF docking scores of compounds docked against XDH (PDB code: 1n5x), the distance of the hydrogen bonds between the compounds and the amino acid residues of XDH, the quantitative identification of the detected hydrogen bonds order by MOPAC 2000, and RMSD of the docked inhibitors from the embedded, experimental ligand

Compound[a]	Docking score (kcal/mol)	Hydrogen bonds between compounds and amino acids			Bond order MOPAC (length Å)	RMSD (Å)[b]
		Atom of compound	Amino acid	Distance (Å)		
Allopurinol	−88.04	N_9–H	O(OE1) of Glu 802	1.88	0.014	4.51
Oxipurinol	−82.16	N_3–H	O(OE1) of Glu 802	1.79	0.032	3.94
		C_6–Oxo	HN of Thr 1010	1.74	0.030	
3b	−80.59	C_4–NH	O(OE1) of Glu 802	1.77	–[c]	2.63
3e	−74.0	N_1–N	HO of Ser 876	2.20	–	2.41
3g	−95.24	C_4–NH	O(OE1) of Glu 802	1.61	0.045	1.02
		C_6–Oxo	HN of Thr 1010	2.17	–	
3h	−89.69	C_6–Oxo	HO of Ser 876	2.01	–	0.80
		p–F	HN(HE) of Arg 880	2.17	–	
3i	−100.38	N_1–NH	OH of Thr 1010	2.10	–	0.47
		N_1–N	HO of Thr 1010	2.10	–	
3p	−95.70	*p*–CO	HN(HH2) Arg 880	2.19	–	1.20
		p–COO	HN of Ala 1079	1.87	0.012	
3q	−97.41	*p*–OH	O of MOS[d]	2.17	–	1.01
3r	−101.79	N_5–N	HO of Ser 876	1.99	0.011	1.66
4a	−103.37	N_6–H	OH of Thr 1010	2.03	0.014	3.70
		C_5–Oxo	HN of Thr 1010	2.12	–	
4b	−101.94	C_5–Oxo	HN of Thr 1010	2.12	–	3.27
		C_5–Oxo	HN of Val 1011	2.11	–	
		N_6–N	HN of Thr 1010	1.79	0.012	
4c	−104.91	N_6–H	OH of Thr 1010	2.08	0.010	2.56
4f	−126.61	N_6–N	HN of Thr 1010	2.14	–	1.30
4g	−119.94	N_6–N	HN of Thr 1010	2.04	–	1.87
		C_5–Oxo	HN of Thr 1010	2.10	–	
		C_5–Oxo	HN of Val 1011	1.65	0.031	
4h	−107.19	*p*–F	HN(HE) of Arg 880	1.57	0.043	0.80
4k	−114.33	C_5–Oxo	HN of Thr 1010	1.70	0.034	2.64
4n	−110.59	C_5–Oxo	HN(HT) of Asn 768	2.11	–	2.01
4s	−129.97	C_5–Oxo	HN of Val 1011 HN of Thr 1010	2.07	0.014	1.76
		C_5–Oxo		1.58		

[a] Their corresponding $IC_{50's}$ are mentioned in Table 1

[b] Root mean square deviation

[c] Hydrogen bond is not identified by Mopac

[d] Dioxothiomolybdenum

affinity of the ligand into the target site. Upon the CAChe docking of the tricyclic 7H-pyrazolo[4,3-e]-1,2,4-triazolo [1-5-c]pyrimidin-5(6H)one analog (**4s**; IC_{50}: 0.037 μM) into XDH (1n5x), it exhibited a docking score of −129.97 kcal/mol. And it was bound with two H-bonds between the C_5–oxo group and the Val 1011 Thr1010 hydrogens as shown in Fig. 6. The latter was identified quantitatively by using MOPAC.

Both of the bicyclic and tricyclic inhibitors (**3p**; IC_{50}: 0.399 μM and **4i**; IC_{50}: 0.070 μM) were docked against XDH (1v97) by using the CAChe-PMF scoring function as shown in Fig. 7a and b, respectively. They revealed docking scores of −93.74 and −117.54 kcal/mol with three H-bonds (with Glu 802 and Thr 1010, and with Thr 1010), respectively. Compound **4i** was located surrounded by the helix RA and sheet AP of the backbone of the protein

Table 3 The best docking results based on the PMF docking scores of compounds docked against XDH (PDB code: 1v97), the distance of the hydrogen bonds between the compounds and the amino acid residues of XDH, the quantitative identification of the detected hydrogen bonds order by MOPAC 2000, and RMSD of the docked inhibitors from the embedded, experimental FYX-051 ligand

Compound[a]	Docking score (kcal/mol)	Hydrogen bonds between compounds and amino acids			Bond order MOPAC (length Å)	RMSD[b] (Å)
		Atom of compound	Amino acid	Distance (Å)		
Allopurinol	−87.20	C_6–OH	NH(HH2) of Arg 880	1.86	0.051	3.99
Oxipurinol	−86.87	N_3–H	O(OE1) of Glu 802	1.78	0.056	4.45
		N_9–H	O of MOS[c]	1.68	0.052	
3b	−84.42	C_4–NH	O(OE1) of Glu 802	1.86	0.029	2.42
		C_6–Oxo	HO of Thr 1010	2.13	–[d]	
3e	−93.05	N_1–N	HN of Thr 1010	2.00	0.011	2.40
		N_2–N	HO of Thr 1010	2.05	0.010	
3f	−107.78	C_6–Oxo	HO of Thr 1010	1.97	–	1.05
		N_4–NH	O(OE1) of Glu 802	2.12	0.012	
3g	−102.56	C_4–NH	O(OE1) of Glu 802	1.89	0.035	1.71
		C_6–Oxo	HO of Thr 1010	2.08	–	
3h	−108.06	C_6–Oxo	HN of Thr 1010	1.75	0.032	1.50
		C_6–Oxo	HN of Val 1011	2.18	–	
		C_6–Oxo	HO of Thr 1010	2.07	–	
		N_7–N	HN of Thr 1010	2.44	–	
3i	−104.31	N_4–NH	O(OE1) of Glu 802	1.89	0.024	1.38
		C_6–Oxo	HO of Thr 1010	2.03	–	
3j	−98.32	C_6–Oxo	HO of Thr 1010	1.88	0.015	1.45
3k	−102.86	N_4–NH	O(OE1) of Glu 802	2.00	0.023	1.44
		C_6–Oxo	HO of Thr 1010	1.89	0.011	
3l	−102.89	N_4–NH	O(OE1) of Glu 802	2.02	0.021	1.35
		C_6–Oxo	HO of Thr 1010	1.86	0.014	
3p	−93.74	N_1–N	HN of Thr 1010	2.08	–	0.32
		N_2–N	HO of Thr 1010	2.14	–	
		N_4–NH	O(OE1) of Glu 802	1.90	0.025	
3q	−108.75	C_6–Oxo	HN of Thr 1010	1.84	0.020	1.31
		C_6–Oxo	HN of Val 1011	1.98	–	
4a	−104.58	C_5–Oxo	HN (HE) of Arg 880	2.06	–	3.06
4b	−106.07	C_5–Oxo	HO of Thr 1010	2.14	–	2.65
4d	−113.68	C_5–Oxo	HO of Thr 1010	2.15	–	0.92
4e	−120.92	C_5–Oxo	HO of Thr 1010	2.19	–	1.24
4i	−117.54	C_5–Oxo	HO of Thr 1010	1.61	0.031	1.29
4j	−121.11	C_6–Oxo	HN of Thr 1010	2.09	–	1.77
		C_6–Oxo	HO of Thr 1010	2.10	–	
4k	−121.99	C_5–Oxo	HO of Thr 1010	2.05	–	1.69
4q	−116.81	*p*–OH	NH(HH2) of Arg 880	2.16	–	1.24
4s	−132.40	C_5–Oxo	HO of Thr 1010	1.96	–	0.62

[a] Their corresponding $IC_{50's}$ are mentioned in Table 1

[b] Root mean square deviation

[c] Dioxothiomolybdenum

[d] Hydrogen bond is not identified by Mopac

structure and its N_8–N atom was oriented closer to MOS moiety within the distance of 3.59 Å. The docking location of these inhibitors is characteristic in a sense that it exhibits their ability to block the substrate binding into the Mo-pterin active moiety of XDH, demonstrating that they are good candidates as XO inhibitors.

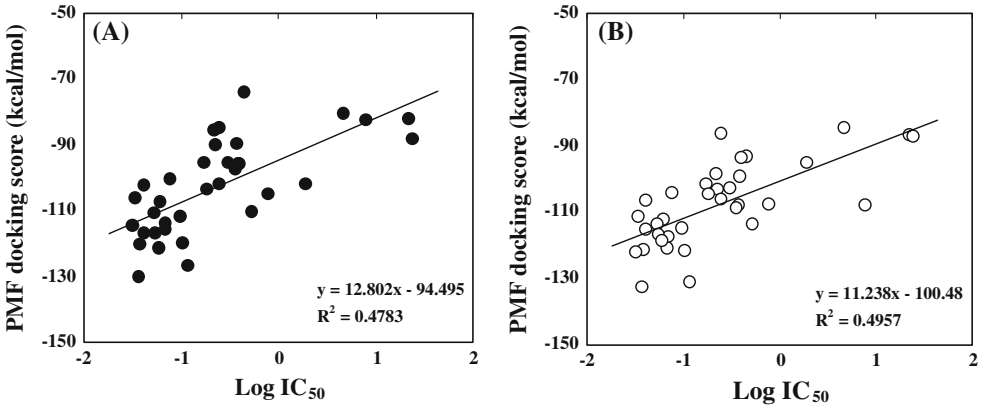

Fig. 4 A correlation feature between PMF-docking scores and logIC_{50} of pyrazolopyrimidines and pyrazolotriazolopyrimidine-idine docked into the active sites of XDH. a and b Represent 1n5x and 1v97, respectively. A reasonable distribution linearity of points on the regression line was observed

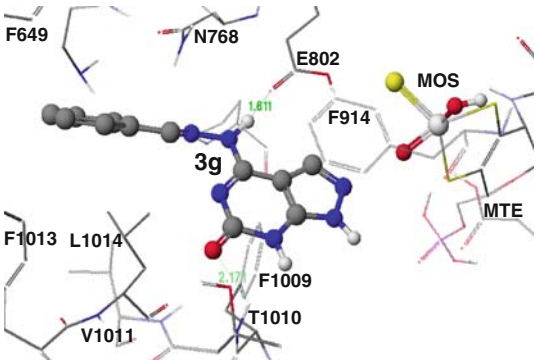

Fig. 5 The binding affinity of the docked bicyclic pyrazolopyrimidine (**3g**, colored by elements, *ball* and *stick*) against XDH (1n5x) using CACheche 6.1.10. It was oriented near the MOS moiety, forming two hydrogen bonds involving Glu 802 and Thr 1010 (shown in *green dotted lines*)

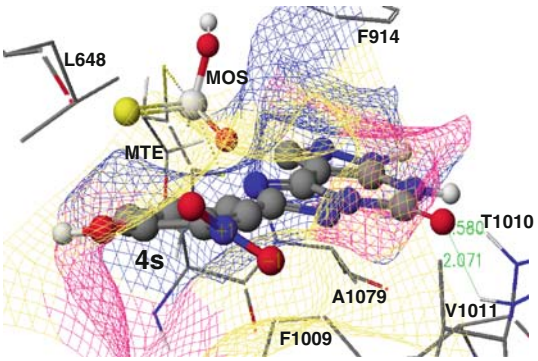

Fig. 6 Interaction of the pyrazolotriazolopyrimidine (**4g**, colored by element, *ball* and *stick*) with the residues lining the access channel to the Mo-pterin moiety of XDH (1n5x). Compound **4s** located within its adjacent surface pocket was oriented closer to the MOS moiety by its N_8–N within 3.15 Å, forming two hydrogen bonds with Thr 1010 and Val 1011

There was no significant difference between the docking modes of allopurinol and oxipurinol. Both of them revealed similar docking scores against XDH (1n5x); −88.04, −82.16 kcal/mol, and against XDH (1v97); −87.20 and −86.87 kcal/mol, respectively. These computer-simulated scores are fairly in good agreement with their experimental in vitro XO inhibitory activities (IC_{50}: 24.3 and 22.1 μM).

TEI-6720, an extremely potent inhibitor of xanthine oxidoreductase (IC_{50}: 0.0014 μM), upon its docking against XDH (1n5x) using CACheche 6.1.10, presented a docking score of −109.17 kcal/mol with one hydrogen bond involving Thr1010 confirmed by MOPAC [36]. A good correlation was observed between this result and the result of the experimental biological activity assay. Docking performances of 6-chloropyrazolopyrimidines (**1a–f**) and 4,6-bis-aldehydedrazone analogs (**2b–f**), using the PMF-scoring function against XDH (1n5x and 1v97) revealed outcomes with poor binding affinities. That is, compounds **2b–f** exhibited meager binding scores (−71.65 to +116.44) and (−77.94 to −38.65) kcal/mol when docked against XDH (1n5x and 1v97).

In this study, additional compounds were investigated as our potentially active XO inhibitors by docking against XDH. These compounds include *β*-naphthol as a negative control, uric acid as its main toxic metabolite of allopurinol, and salicylic acid as an in vitro competitive inhibitor against the substrate binding into the Molybdenum active site. Upon docking these compounds against XDH (1n5x and 1v97) by using CACheche 6.1.10, all of them exhibited the lowest binding affinities, that is, poor docking scores (−64.75 and −67.01), (−80.43 and −84.18), and (−66.35 and −67.18), kcal/mol. *β*-naphthol did not exhibit any hydrogen bond within the binding site, whereas uric acid exhibited one or two hydrogen bonds, and salicylic acid, two to four.

Structure activity relationship (SAR)

Another objective of this study is to investigate the structure–activity relationships (SAR) to find out the correlation between the different structural features of each ligand and the different parameters including the experimentally measured xanthine oxidase inhibitory activity (IC_{50}) and

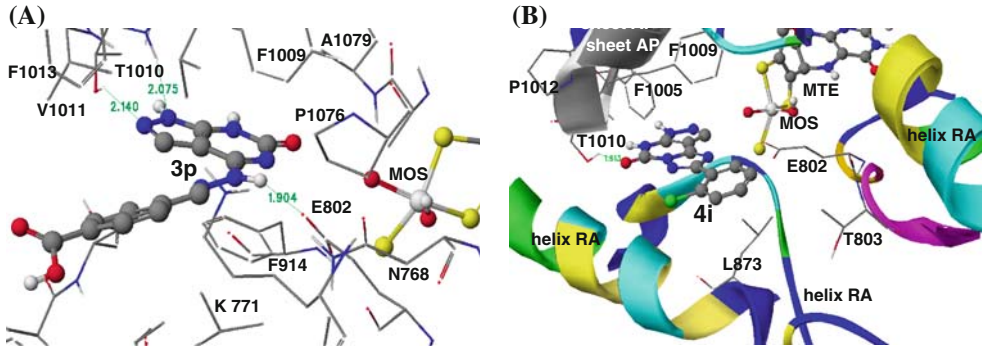

Fig. 7 Inhibitors **3p** and **4i** were docked against XDH (1v97) using CAChe 6.1.10. In a **3p** exhibited 3 H-bonds with Glu 802 and Thr 1010 close to the MOS moiety by the distance of 4.13 Å. In b **4i** exhibited one H-bond involving Thr1010 and it was located between the helix RA and the sheet AP, closer by its N_8–N within the distance of 3.59 Å to the MOS moiety. XDH is shown as solid backbone ribbon

the binding free energy (ΔG_b), calculated by AutoDock. Our SAR study revealed the following findings:

1. The order of potency based on the obtained binding energies can be arranged in an ascending order as follow:

Pyrazolotraizolopyrimidines (**4**) > pyrazolopyrimidines (**3**) > allopurinol and oxipurinol > 6-chloro derivatives (**1**) > 4,6-bis-aldehydehydrazone derivatives (**2**).

$IC_{50's}$ and binding free energies of compounds (**4a–s**) are 0.032 and 0.782 μM, and −11.78 kcal and −8.86 kcal/mol. Seventy-nine percent of them exhibited ΔG of less than −10.0 kcal/mol. $IC_{50's}$ and binding free energies of compounds (**3a–r**) are 0.077 μM and −7.89 μM, and −11.85 and −7.72 kcal/mol. Seventy-nine percent of them exhibited ΔG of less than −9.23 kcal/mol. $IC_{50's}$ and binding free energies of allopurinol and oxipurinol are 24.3 and 22.1 μM, and 7.39 and −7.54 kcal/mol. Those of compounds (**1** and **2**) are greater than 10 μM, and −8.04 to −9.78 kcal/mol and −8.21 to −9.52 kcal/mol.

2. C_6–oxo or C_5–oxo groups of bicyclic pyrazolopyrimidines and tricyclic pyrazolotriazolopyrimidines are essential in securing a good binding affinity as they are the major moiety involved in hydrogen bonding within the binding site. Missing of this oxo group in compounds **1** and **2** lead to a loss of activity (IC_{50} > 10 μM). This loss of activity resulted from an inappropriate fitting of compound **1** and compound **2** into the binding site. The first analog group have 6-Chloro atom which is weakly involved in hydrogen bond, while the second analog group have 4,6-bis-aldehydedrazone moieties which consist of so bulky structures as to be rejected from the binding pocket.
3. The potency of pyrazolotriazolopyrimidine analogs were ca. five times more than that of pyrazolopyrimidine analogs. This is mainly attributed to planarity of the former tricyclic structure which exhibited a tight fitting within the binding pocket in consequence of aromatic/aromatic surface interaction (van der Waals) with the surrounding phenylalanine amino acids, where its tricyclic moiety was sandwiched between Phe 914 and Phe 1009 as shown in Fig. 6.
4. XO inhibitory activities of 4-arylmethylidenehydrazinopyrazolopyrimidine analogs (**3g–q**, IC_{50}: 0.077–0.399 μM) and 2-aryl substituted pyrazolotriazolopyrimidine analogs (**4g–s**, IC_{50}: 0.032–0.0.098 μM) were ca. 10 times more than those of their 4-alkyl substituted analogs. It is clearly shown that the aryl fragment is deeply embedded and accommodated into the hydrophobic region exhibiting an electrostatic surface attraction and hydrophobic interactions with Leu 648, Lys 771, Leu 873, and Leu 1014 as shown in Fig. 8 for compound **4r** (IC_{50}: 0.060 μM, ΔG_b: −11.19 kcal/mol). The alkyl substituted derivatives **3b**,**e**,**f** (IC_{50}: 0.45–7.89 μM) and **4a–f** (IC_{50}: 0.069–0.782 μM) are less likely to fit into this non polar region especially for the derivatives carrying short hydrocarbon chains as shown in compounds **3b** (IC_{50}: 4.67 μM, ΔG_b: −8.07 kcal/mol).and **4c** (IC_{50}: 0.782 μM, ΔG_b: −9.33 kcal/mol).
5. 2-Alkyl substituted pyrazolotriazolopyrimidine analogs exhibited different types of XO inhibitory activities based on the length of the carbon chain. The higher activity among alkyl analogs was demonstrated; C: 2< or >4. This relationship between the potency and the number of carbon atoms can be displayed as an inverted bell curve with the peak optimum at seven carbons. Therefore, compounds with 2-*n*-C_7H_{15}(**4e**) exhibited the lowest IC_{50} of 0.069 μM and the excellent AutoDock binding affinity (ΔG_b: −10.84 kcal/mol) with two hydrogen bonds involving Arg 880 and Ala 1079 as shown in Table 1.
6. The most potent 2-aryl pyrazolotriazolopyrimidine derivatives (**4g–s**) showed a slight variation depending on the substituent on the aryl moiety at C-2 position.

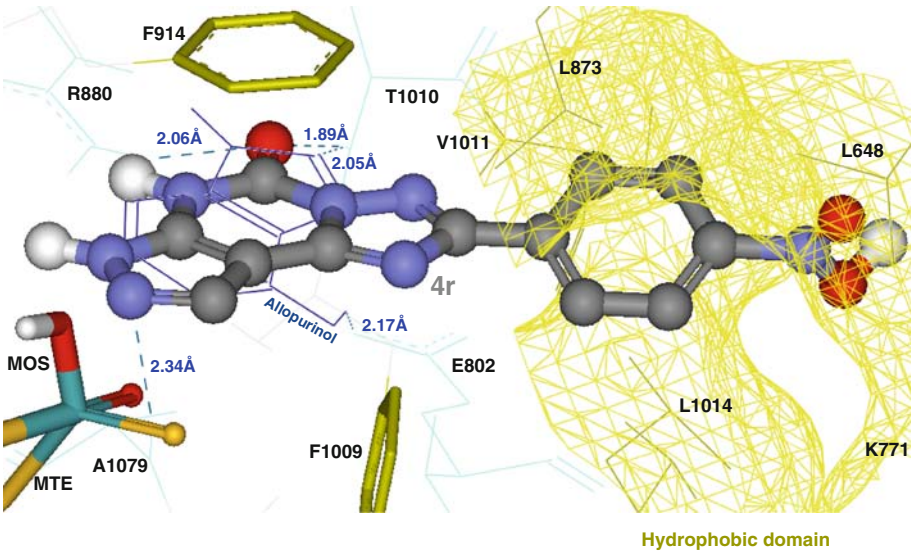

Fig. 8 Mode of interactions of allopurinol (*indigo*, *line*) and compound **4r** (*ball* and *stick*, colored by elements) docked into the binding site of PTK (1t46) using AutoDock 3.05. They exhibited two to three hydrogen bonds (shown in *green dotted lines*), respectively. The hydrophilic domain of amino acid residues, where the hydrogen bonds were formed, are shown in *cyan colored lines*. The aryl side chain of ligand **4r** is deeply accommodated into the hydrophobic domain of the surrounding amino acid residues (shown in *yellow* colored wire mesh surface)

This was confirmed also by AutoDock ΔG_b as shown in Table 1. The unsubstituted phenyl derivative **4g** (IC_{50}: 0.103 μM, ΔG_b: −10.53 kcal/mol) exhibited the lowest potency among their analogs. Also positional isomerism of the aryl substitution affected the compound's activity. The less bulky substitution at *m*- and *p*- and the lipophilic substituents such as *m* and *p*–Cl, Br and Me showed not only the lowest IC_{50} but also the low binding free energies. Examples of such compounds are **4j** (*m*–Cl, IC_{50}: 0.038 μM, ΔG_b: −11.21 kcal/mol), **4k** (*p*–Cl, IC_{50}: 0.032 μM, ΔG_b: −10.97 kcal/mol) **4l** (*p*–Br, IC_{50}: 0.034 μM ΔG_b: −11.08 kcal/mol), and **4m** (*p*–Me, IC_{50}: 0.041 μM, ΔG_b: −10.98 kcal/mol).

Mode of binding of pyrazolopyrimidine derivatives as XO inhibitors against XDH

The mechanism of allopurinol inhibition of XDH has been studied in details by Massey et al. [37]. They found that the enzyme oxidizes allopurinol to oxypurinol, which then in turn coordinates tightly to the pterin-bound Mo(IV) ion, preventing further catalysis. Therefore, the reaction mechanism involves a nucleophilic attack at the deprotonated Mo–OH on the C-2 position of a substrate. The types of amino acids involved in ligand–enzyme binding were reported by many investigators [29, 30, 38]. The pharmacophoric moiety of pyrazolopyrimidine derivatives is similar to that of substrates such as allopurinol and oxipurinol, strongly suggesting that a similar mode of interaction might also be seen in different pyrazolopyrimidines. The hydroxylation at carbon (C_3) of the pyrazole ring of these pyrazolopyrimidine derivative is expected to take place because they were located closer to the Mo-pterin moiety by their N_2–N in pyrazolopyrimidines or N_8–N pyrazolotriazolo–pyrimidines, where numerous hydrogen bonds as well as hydrophobic interactions with the protein matrix were observed in docking against XDH.

As far as the types of amino acid residues are concerned for the hydrogen-bond formation, Arg 880 and Thr 1010 are involved more frequently than others. This also indicates that Arg 880 and Thr 1010 play an important role in the metabolic process in binding of ligands within the active site. The mechanism of this process may be due to the polar hydrogens of their acetamidine (NH) and 3-OH moieties, being a perfect hydrogen donor's candidate. Glu-802, Ser-876, Val 1011, and Ala-1078 take part in the hydrogen bond formation with relatively less frequency. This information is helpful for our drug design in which the potential drug should interact well with these residues, especially with Arg 880 and Thr 1010.

The docking conformation of several compounds were observed in the solvent channel between helix RA and sheet AP (Fig. 7b) that provides access to the active site of the Mo-pterin moiety. They were located closer to the Mo-pterin moiety by their N_2–N in pyrazolopyrimidines or N_8–N in oxipurinol and pyrazolotriazolopyrimidines within the distances of 1.68–4.47 Å as shown in Figs. 5, 6, 7a, and b for compounds **3g** (3.45 Å), **4s** (3.15 Å), **3p** (4.13 Å), and **4i** (3.59 Å), respectively. N_8–N and C_2 atoms of allopurinol and oxipurinol, are the closest atom to Mo-pterin moiety within the distances of 3.5 and 4.00 Å, respectively. A few ligands exhibited direct H-bonds with oxo-group of the MOS moiety. Those are **3q** and oxipurinol within the distances of 2.17 and 1.68 Å upon docking against XDH (1n5x and 1v97), respectively.

The planar pyrazolopyrimidine ring of all the docked ligands exhibited an aromatic/aromatic surface interaction with the surrounding phenylalanine amino acids, as shown

in Fig. 8. As a whole, it was sandwiched between Phe 914 within 3.45 Å and Phe 1009 within 3.88 Å in distances. This surface interaction can also be observed in Figs. 5, 6, and 7a for ligands **3g**, **4s**, and **3p**, respectively. In all of this interaction the planar pyrazolopyrimidine ring was aligned parallel to the ring of Phe 914, whereas the phenyl ring of Phe 1009 interacted perpendicularly with the center of the pyrimidine ring with the closest access distance of 3.25 Å. By this model of binding of pyrazolopyrimidines with the active site moieties, many ligands were oriented by their N_2–N (bicyclic ligands) or N_8–N (tricyclic ligands) near to the dioxothiomolybdenum (MOS) moiety within the distance of 1.87 Å, as shown in Fig. 8. Hence this binding mode supports the proposed mechanism of action illustrated in Fig. 9 for ligands to be able to form a covalent bond with the molybdopterin. In addition, the phenyl side chain of the docked ligands exhibited hydrophobic–hydrophobic interaction within the hydrophobic surrounding residues including Leu 648, Leu 873, Lys 771, Val 1011 and Leu 1014 within the distances of 3.20–4.75 Å. The phenyl side chain of the docked ligand was surrounded by the alkyl moieties of these amino acids as shown in Fig. 8. This interaction incurs the orientation of the phenyl side chain of the docked ligands into its active site. However, these hydrophobic–hydrophobic interactions are of less significance in ligand binding to the active site, where the binding energy is estimated to be 0.37 kcal/mol, about 10 times weaker than that of hydrogen bonds whose energies range from 1 to 7 kcal/mol. The more hydrogen bonds are formed the better the docked ligands are kept within the active site pocket.

The C_6–oxo and N_7–H of pyrazolopyrimidines (**3**) and C_5-oxo and N_6–H of pyrazolotriazolopyrimidines (**4**) were docked close to the backbone amide hydrogen (NH) or the hydroxyl side chain of Thr1010 within the distances of 1.58–2.49 Å which are common lengths involved in hydrogen bonding. These moieties of ligands (**3** and **4**) were involved in many hydrogen bonds within the distances of 1.57–2.27 Å from the hydrogen atom (HH22) of the guanidinium group of Arg 880, which also bound to the substituents of the aryl side chain. The 4-hydrazine hydrogen of the bicyclic pyrazolopyrimidines bound also to the oxygen of carbonyl group of the carboxylate residue of Glu 802 within the distances of 1.61–2.12 Å.

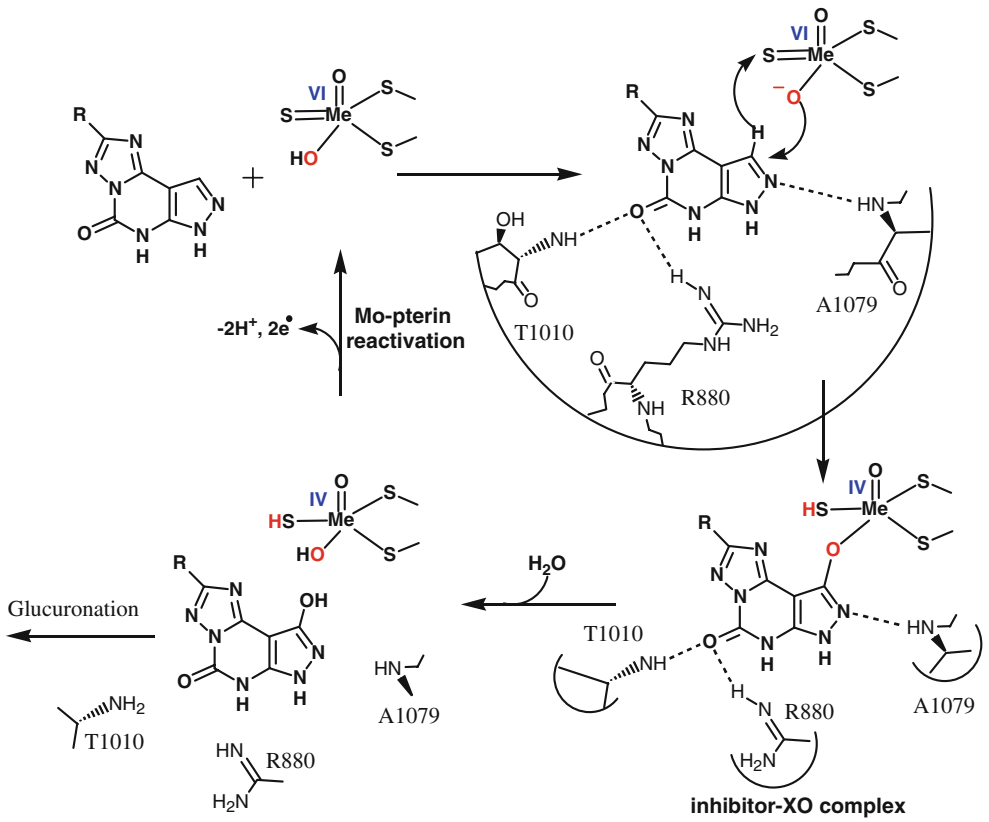

Fig. 9 The proposed mechanism of XDH inhibition initiated by base-assisted nucleophilic attack of Mo–OH on pyrazolopyrimidine ligands, with subsequent hydride transfer to produce the inhibitor—XO complex. Consequently, the Mo-pterin oxidative reactivation occurs by two electron transfers via two Fe_2S_2 clusters to the isoalloxazine ring of FAD (reference 15)

Conclusions

In this study, we applied two scoring functions of the binding interaction, that is, AutoDock 3.05 and the PMF-knowledge-based scoring approach of CACHe 6.1.10; where several aspects of their performance were compared including binding energies, hydrogen bonding, and RMSD from the crystal bound ligand. The preliminary docking validation of the crystal ligand TEI-6720 of XDH (1n5x) into its binding site demonstrated that the obtained success rates of AutoDock 3.0.5 and CACHe 6.1.10 were fairy well and identical in both functions. Hence the RMSD of the top ranking conformations were almost equal with the distances of 0.633 and 0.625 Å, and the AutoDock binding free energy (ΔG_b) and the PMF-CACHe docking score were −10.34 and −109.17 kcal/mol, respectively.

Upon application of these scoring functions for docking of the 4-substituted 4-alkylidenehydrazino- or 4-arylmethylidenehydrazino-1H-pyrazolo[3,4-*d*]pyrimidines (**3**) and the 2-substituted 7H-pyrazolo[4,3-*e*]-1,2,4-triazolo[1,5-*c*] pyrimidines (**4**) against XO, the overall correlation between the binding energy or the docking score and the reported in vitro XO inhibitory activities was fairly good with oxipurinol, allopurinol, TEI-6720, salicylic acid as a positive control, *β*-naphthol, and uric acid as a negative control. However, the free energy implemented in the AutoDock program revealed a better correlation with the experimental results than that obtained by PMF-docking score implemented in the CACHe 6.1.10. As the former function revealed correlation coefficients (R^2) of 0.694 involving 35 ligands and 0.769 for 33 ligands docked into XDH (1n5x), while the later exhibited correlation coefficients (R^2) of 0.478, involving 35 ligands and 0.542 for 33 ligands.

There was no significant difference between the results obtained by docking against XDH (1n5x) and XDH (1v97) using CACHe 6.1.10, where those revealed the correlation coefficients (R^2) of 0.478 and 0.496 involving 35 ligands (n), and 0.542 and 0.613 involving 33 ligands, respectively. These observations indicates that Muggue's PMF approach involved in CACHe 6.1.10 performs less favorably than AutoDock 3.05. It is noteworthy that AutoDock did not reveal any drastic "false negatives" nor 'false positives' results upon correlating its binding energy with log IC_{50}. These ligands when docked into the active site of bovine milk XDH were bound in the narrow channel leading the ligands to the molybdenum center of the enzyme. Hence, these ligand molecules filled the entire pocket thereby inhibiting the activity of the enzyme simply by preventing the substrate from entering and binding to the active site pocket.

The docked pyrazolopyrimidine ligands generated many hydrogen bonds at the binding site of XDH (1n5x and 1v97) involving such amino acid residues as Arg 880 and Thr 1010 in addition to Lys 771, Glu 802, Ser 876, and Ala 1079. It is proposed that the mode of interaction of the ligands with the enzyme (XDH) would be via direct coordination to the molybdenum ion followed by hydroxylation of the pyrazolopyrimidine moiety. This proposal is based on the fact that (1) there are a structural similarity of the nucleus of the ligands including allopurinol and oxipurinol in this study, (2) ligands were docked closer to the Mo-pterin moiety within the distances of 1.68–4.47 Å, (3) many hydrogen bonds as well as hydrophobic interactions at the binding site were generated. A study on SAR of the forementioned compounds indicates that C_6–oxo or C_5–oxo groups of bicyclic and tricyclic pyrazolopyrimidine is essential in securing a good binding affinity leading to the hydrogen bonding.

The higher XO inhibitory activity was shown with the following structural features: (1) the pyrazolotraizolopyrimidines over the pyrazolopyrimidine analogs, (2) 4-arylmethylidenehydrazino pyrazolopyrimidines and 2-aryl substituted pyrazolotriazolopyrimidines over the alkyl derivatives, (3) 2-alkyl substituted pyrazolotriazolopyrimidine analogs of carbon chain length within 2< or >4, and (4) *m* and *p*-less bulky, lipophilic substitution (e.g. *m* and *p*–Cl, Br or Me) of the aryl moiety.

Experimental

Preparation of the target macromolecule

By using the molecular modeling software CACHe WS Prov.6.1.10 (Fujitsu Limited), and Accelrys Discovery Studio version 1.6., the two 3D coordinates of bovine milk ligand–protein XDH complexes, namely, 1n5x and 1v97 were retrieved from the Brookhaven Protein Data Bank (URL*http://www.rcsb.org/pdb/Welcome.do., accessed on Jan.2006) [29, 30]. They were obtained as an identical dimeric structure (two subunits, chains A and B) of xanthine oxidase. They were simplified to a monomer by deleting chain B. One of the subunits of the enzyme with its cofactors was employed as a search model. The subunit was split into a protein molecule and a ligand molecule TEI and FYX, respectively. All proteins and ligands were saved in PDB format. The molybdenum metal ions (Mo) and cofactor MTE (phosphoric acid mono 2-amino-5,6-dimercapto-4-oxo-3,7,8a,9,10,10a-hexahydro-4H-8-oxa-1,3,9,10-tetraaza-anthracen-7-yl methyl) ester on the protein–ligand interface were left with the protein. The HET (heterogen group i.e. any moiety in the protein other than amino acid groups of the protein) were corrected according to their IUPAC name in PDB. All of the other organic and inorganic cofactors, as well as all the water molecules, were removed. Polar hydrogen atoms were added to both the protein and the ligand. United

atom *Kollman* charges were assigned for the protein. Atom types and bond types of the ligand molecule were inspected and corrected manually.

Preparation of small molecules

The three dimensional (3D) structures of various derivatives of bicyclic pyrazolopyrimidines and tricyclic pyrazolotriazolopyrimidines were drawn by using the chemical modeling software CAChe Pro version 6.1.10. Structures of the small molecules were refined by performing an optimized geometry calculation in mechanics using the augmented AM1 MOZYME geometry. They were assigned as inhibitors for the docking study. Chem 3D ultra 8.0 software [Molecular Modeling and Analysis; Cambridge Soft corporation, USA (2003)], was used for construction of the 3D structures involved in AutoDock. These compounds were energetically minimized by using MOPAC (semi-empirical quantum mechanics) with AM1 MOZYME geometry at 100 iterations and minimum RMS gradient of 0.10.

Docking protocol involving the PMF Scoring function of CAChe WS Prov.6.1.10

The computer docking of flexible ligands into the predefined rigid active site using a genetic docking algorithm (GA) with the PMF-scoring function were performed using CAChe WS Prov.6.1.10 as illustrated in Fig. 10 [25]. Each GA run was executed with a population of 50 chromosomes (set of parameters to define a proposed solution to the problem that the genetic algorithm tries to solve), a crossover ratio of 0.80, a mutation rate of 0.30, an elitism of 7.0, maximum generations of 40,000–160,000, and convergence of 1.0 coca. The local search consisted of 300 maximum iterations at a rate of 0.06. The default values given by the CAChe program were assigned for other miscellaneous parameters.

The modes of interaction of TEI-6720 "2-(3-cyano-4-isobutoxy-phenyl)-4-methyl-5-thiazole-carboxylic acid" ligand into XHD (1n5x) and FYX-051 "4-(5-pyridin-4-yl-1H-1,2,4-triazol-3-yl)pyridine-2-carbonitrile" into XDH (1v97) were used as a standard docked model, both for the selection of the pertinent amino acids at the active sites, and for the calculation of the root mean square deviation (RMSD) of the docked inhibitors. The results were evaluated according to the value of the docking scores, RMSD, and the number of H-bonds between the ligand and the binding site of the enzyme. The characteristics of the detected H-bonds between the docked ligands and the binding site residues were checked by MOPAC 2002 (using AM1 MOZYME geometry) for bond orders, angles and distances of generated H-bonds. Hydrogen-bonds within the distance of 2.5 Å were treated as true H-bonding [39]. The results were also evaluated by comparing the docking and binding affinities of compounds in this study with those of oxipurinol, allopurinol, TEI-67620, salicylic acid as positive control, β-naphthol, and with uric acid as negative control.

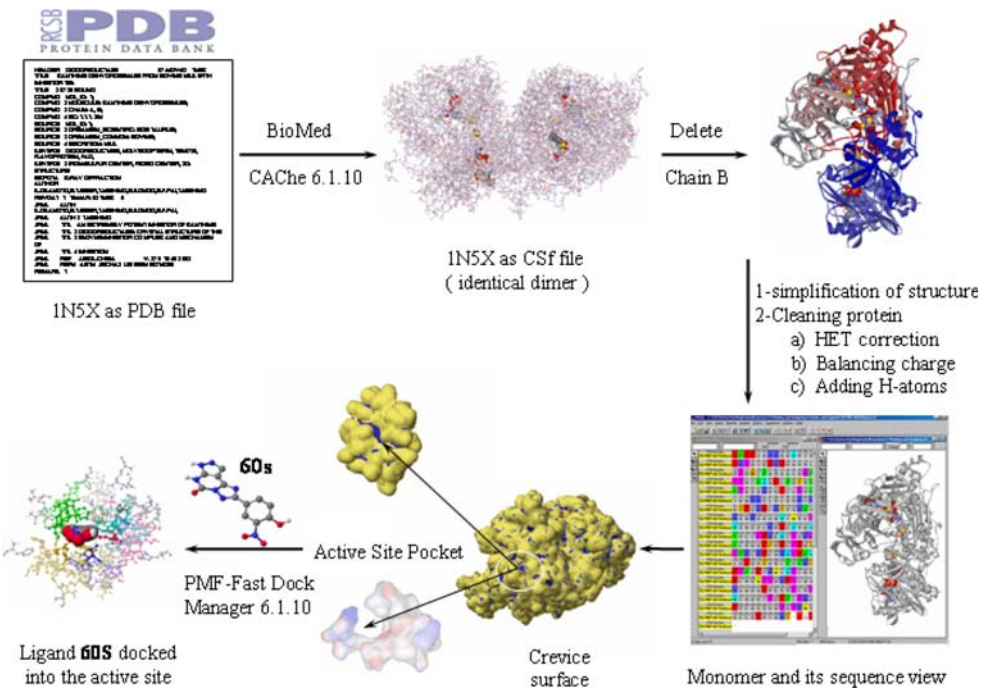

Fig. 10 The experimental in silico drug design protocol from the docking of the ligand into the active site pocket of the downloaded PDB structure

AutoDock scoring function using AutoDock 3.0.5

The AutoDock system (version 3.0.5) was employed to generate an ensemble of docked conformations for each ligand molecule [34]. Of the three different search algorithms offered by AutoDock 3.05, the genetic algorithm with local search (GALS) was applied to the model for the interaction/binding between the target macromolecule and the docked ligand. Each GALS run output a single docked conformation as the final result. Fifty individual GALS runs were conducted to generate 50 docked conformations for each ligand. Each GALS run was performed with a population of 150 chromosomes, a crossover ratio of 0.80, a rate of gene mutation of 0.02, and an elitism ratio of 0.10. During docking, all the rotatable single bonds in the ligand, e.g. sp^3–sp^3 and sp^3–sp^2, were allowed to rotate confirming the flexible docking mode. The size of the docking grid box (x, y, z) was assigned to be 60, 60, and 60 Å which was centered at the experimentally observed position of the ligand. The grid box was large enough to enclose the largest docked inhibitors of the entire test set. The grid spacing inside the docking box was set to be 0.30 Å. The default values were assigned for other parameters. The protein structure was kept rigid during the docking study.

Cluster analysis was performed on the docked results using a root mean square (RMS) tolerance of 0.5 Å. The clusters were ranked from the averaged lowest energy group obtained for the cluster members to the highest. The analysis was carried out for the top 10 docking clusters. The modes of interactions of the experimental ligands, TEI and FYX, within XDH were used as a standard docked model as well as for RMSD calculation. All calculations were carried out on the Linux based machine. The inhibitors were compared based on the best binding free energy obtained among all the docking runs [40].

Molecular modeling and analysis of the binding mode

The conformation with the lowest final docked energy given by AutoDock or CAChe was chosen and analyzed qualitatively based on the location/orientation of the inhibitor in relation to the experimental ligand (TEI and FYX). Each of the selected conformation with significant negative interaction energies was examined and modeled by using Accelrys Discovery Studio version 1.7 [Accelrys Inc, San Diego, CA (2006)]. It was used for evaluation of the mode of interaction, measurement of RMSD, and evaluation of hydrogen bonds in the ligand–receptor interaction. The hydrogen bonds within the distance of 2.5 Å in length and of the angle (θ, between the lone-pair of the acceptor atom, the polar hydrogen, and the donor atom) $\geq 135°$ were considered as a genuine hydrogen bond [41].

Acknowledgments This work was supported in part by Academic Frontier Grants-in-aid of the Ministry of Education, Science and Technology in Japan and we are grateful to the people in charge for the grant assignment.

References

1. Nagamatsu T, Fujita T, Endo K (2000) Perkin 1:33
2. Nagamatsu T, Ukai M, Yoneda F, Brown DJ (1985) Chem Pharm Bull 33:3113
3. Nagamatsu T, Yamasaki H (1995) J Chem Soc Chem Commun 19:2041
4. Nagamatsu T, Yamasaki H, Akiyama T, Hara S, Mori K, Kusakabe H (1999) Synthesis 4:655
5. Nagamatsu T, Fujita T (1999) Chem Commun (Cambridge) 16:1461
6. Sato S, Tatsumi K, Takahashi T (1991) Purine and pyrimidine matabolism in man. Plenum, New York
7. Elion GB, Callahan S, Nathan H, Bieber S, Rundles RW, Hitchings GH (1963) Biochem Pharmacol 12:85
8. Chien S-C, Yang C-W, Tseng Y-H, Tsay H-S, Kuo Y-H, Wang S-Y (2009) Planta Med 75:302
9. Chohan S, Becker MA (2009) Curr Opin Rheumatol 21:143
10. Edwards NL (2009) Rheumatology, vol 48, p 1115. Oxford
11. Haba M, Kinoshita H, Matsuda N, Azma T, Hama-Tomioka K, Hatakeyama N, Yamazaki M, Hatano Y (2009) Anesthesiology 111:279
12. Maitraie D, Hung C-F, Tu H-Y, Liou Y-T, Wei B-L, Yang S-C, Wang J-P, Lin C-N (2009) Bioorg Med Chem 17:2785
13. Mukhopadhyay P, Rajesh M, Batkai S, Kashiwaya Y, Hasko G, Liaudet L, Szabo C, Pacher P (2009) Am J Physiol 296:H1466
14. Murata K, Nakao K, Hirata N, Namba K, Nomi T, Kitamura Y, Moriyama K, Shintani T, Iinuma M, Matsuda H (2009) J Nat Med 63:355
15. Sousa C, Pereira DM, Valentao P, Ferreres F, Pereira JA, Seabra RM, Andrade PB (2009) J Agric Food Chem 57:2288
16. Tan W-J, Xu J-C, Li L, Chen K-L (2009) Nat Prod Res Part B 23:393
17. Xiao J, She Q (2008) Xinxueguan Bingxue Jinzhan 29:622
18. George J, Struthers AD (2008) Cardiovasc Ther 26:59
19. George J, Struthers AD (2009) Vasc Health Risk Manage 5:265
20. Fang J, Seki T, Maeda H (2009) Adv Drug Delivery Rev 61:290
21. Lin H-C, Tsai S-H, Chen C-S, Chang Y-C, Lee C-M, Lai Z-Y, Lin C-M (2008) Biochem Pharmacol 75:1416
22. Prusis P, Dambrova M, Andrianov V, Rozhkov E, Semenikhina V, Piskunova I, Ongwae E, Lundstedt T, Kalvinsh I, Wikberg JES (2004) J Med Chem 47:3105
23. Lin C-M, Chen C-S, Chen C-T, Liang Y-C, Lin J-K (2002) Biochem Biophys Res Commun 294:167
24. Wang R, Lu Y, Wang S (2003) J Med Chem 46:2287
25. CAChe (2000–2004) Work system pro version 6.1.10. Fujitsu Limited, Japan
26. Muegge I, Martin YC (1999) J Med Chem 42:791
27. Muegge I (2000) Perspect Drug Discovery Des 20:99
28. Muegge I (2001) J Comput Chem 22:418
29. Okamoto K, Eger BT, Nishino T, Kondo S, Pai EF, Nishino T (2003) J Biol Chem 278:1848
30. Okamoto K, Matsumoto K, Hille R, Eger BT, Pai EF, Nishino T (2004) Proc Natl Acad Sci USA 101:7931
31. Ferrari AM, Degliesposti G, Sgobba M, Rastelli G (2007) Bioorg Med Chem 15:7865
32. Warren GL, Andrews CW, Capelli A-M, Clarke B, LaLonde J, Lambert MH, Lindvall M, Nevins N, Semus SF, Senger S, Tedesco G, Wall ID, Woolven JM, Peishoff CE, Head MS (2006) J Med Chem 49:5912

33. de Graaf C, Oostenbrink C, Keizers PHJ, van der Wijst T, Jongejan A, Vermeulen NPE (2006) J Med Chem 49:2417
34. Morris GM, Goodsell DS, Halliday RS, Huey R, Hart WE, Belew RK, Olson AJ (1998) J Comput Chem 19:1639
35. Meng EC, Kuntz ID, Abraham DJ, Kellogg GE (1994) J Comput Aided Mol Des 8:299
36. Osada Y, Tsuchimoto M, Fukushima H, Takahashi K, Kondo S, Hasegawa M, Komoriya K (1993) Eur J Pharmacol 241:183
37. Massey V, Edmondson D (1970) J Biol Chem 245:6595
38. Enroth C, Eger BT, Okamoto K, Nishino T, Nishino T, Pai EF (2000) Proc Natl Acad Sci USA 97:10723
39. Stewart JJP (1990) J Comput Aided Mol Des 4:1
40. Bolstad ES, Anderson AC (2009) Proteins 75:62
41. Liang S, Meroueh SO, Wang G, Qiu C, Zhou Y (2009) Proteins 75:397